Volumetric Calibration Refinement using masked back projection and image correlation superposition

Christoph Brücker[1],*, David Hess[2], Bo B. Watz[2]
1: Dept. of Aeronautical Engineering, City University London, Great Britain
2: Dantec Dynamics AS, Denmark
* Correspondent author: Christoph.Bruecker@city.ac.uk

Keywords: PIV processing, Camera calibration, 3D-PIV, TOMO-PIV, Calibration, Calibration Refinement

ABSTRACT

This paper deals with a new, reconstruction based, approach of refining a volumetric calibration. The technique is based on a 2D cross-correlation between particle images on the sensor plane with a planar back projection from a tomographic reconstruction in the same sensor plane to determine potential disparities between the initial camera calibration and the measurement. Additive superposition of the correlation maps from different sets or particle images allows reducing the influence of noise and ghost particles such that the systematic errors in the calibration can be corrected. The different sections describe the theory, the principle processing steps and the convergence of the procedure. Furthermore, the concept is proven by simulating the entire process of the measurement chain, with the help of a synthetic comparison. The results show that disparities of over 9 pixels could be corrected to an average of below 0.1 pixels during the refinement steps. Finally, the technique demonstrates it´s potential to measured data, where the numbers of outliers in the raw results are reduced after the volumetric calibration refinement.

1. Introduction

As a known fact, a proper camera calibration is key to a successful volumetric measurement. Changes of the camera scene typically requires a new calibration, therefore an unintentional movement of one or more cameras after initial calibration may lead to errors if the calibration functions are not up-dated accordingly. On the other hand, the mapping functions between the world and image coordinates (and the inverse of those) representing the mathematics of the calibration process could be affected by errors in the target coordinates, modifications in the optical properties along the viewing directions and errors in the image processing routines to determine the mapping functions. Moreover, the approximation of the camera models such as pinhole or lens distortion functions may not be ideal in all aspects for the actual recording situation. The consequence of all of this a reduced accuracy of the measurement or even a complete

failure. This is especially important in voxel-based reconstructions of particle-filled volumes as the reconstruction quality largely depends on the calibration accuracy.

Consider a standard multi-camera arrangement for volumetric Particle Image Velocimetry such as 3D Particle Tracking (3D-PTV) or Tomographic PIV (Tomo-PIV) see Fig. 1a. The minimum of three cameras can view the scene in different planes or - for simplification - in the same plane but from different angular displacements (Fig. 1b) or translational displacements. A particle in the world coordinate system is then projected into the image plane according the mapping functions, describing the transfer from world to image coordinates. The mapping functions are typically calculated from calibration images of targets in the volume whose world coordinates are given a-priori. For reconstruction of the particle field in the volume, one way is to calculate the inverse of the mapping functions describing the lines of sights (LOS) for each pixel of each camera. It allows then to calculate the tomographic MART- or SMART-type of voxel reconstructions, or in the simplest way, to use the shape-of-silhouette method (SOS) in the voxel space. There, the particles are reconstructed as clusters of voxels with the center of gravity crossed by all LOS originating from the particle image centers in the image planes. Errors introduced in the calibration procedure and/or changes in the camera positions between measurement situation and calibration may lead to unsuccessful reconstructions when using the original mapping function obtained in the calibration. Consequently, disparities in the images planes need to be corrected in the calculation of the mapping functions if the LOS originating from image centers corresponding to the same particle should again come to crossing of each other in the center of gravity in the reconstructed volume.

In practice, this crossing is never accurate enough to hit exactly the center of gravity, even with perfect mapping. This, in addition to other issues depending on spatial resolution, number of cameras, viewing angles and noise sources, leads to non-perfect reconstructions of the particles. As a practical guide, Arroyo and Hinsch (2008) recommended a disparity below 0.4 pixels to ensure that a typical tracer particle of 3px diameter in the image plane is still reconstructed as a compact cluster in the voxel space. In fact, these 0.4 pixel of uncertainty can already have a significant influence on the 3D shape of reconstructed particles. Therefore, in Volumetric Particle Image Velocimetry the calibration procedure must aim to get the disparity in all image planes below a certain threshold. In 2008, Wieneke suggested to calculate disparity maps based on comparison of triangulated particle coordinates and particle images in the image planes, which can be used to correct the calibrations. The present work represents an alternative approach, which

uses iterative voxel-field reconstructions and back-projections to calculate the disparity maps. Therefore, particle images are reconstructed using MinLos or SMART (see Atkinson and Soria 2008) and small subsections of the volume are then back-projected to the image planes and compared with the local image pattern in the original images. This is done stepwise selecting the sections along a 3D grid covering the box-size of the reconstructed volume. Disparities are calculated from several realizations of particle recordings, which allow to remove the influence of ghost particles and noise from the final results.

2. Calibration Refinement Method

Assuming a situation of a three-camera set-up with angular displacement (cam#1 -45°, cam#2 0°, cam#3 +45°) in one plane and a misalignment of the left-most camera in form of a shift in the camera plane. The imaging system is such that all LOSs are straight lines and perpendicular to the image plane (telecentric approximation). The original camera calibration induces then a shift of the LOSs in direction of the red arrow (see Fig. 1b), equivalent to a virtual shift of the particle image in this camera.

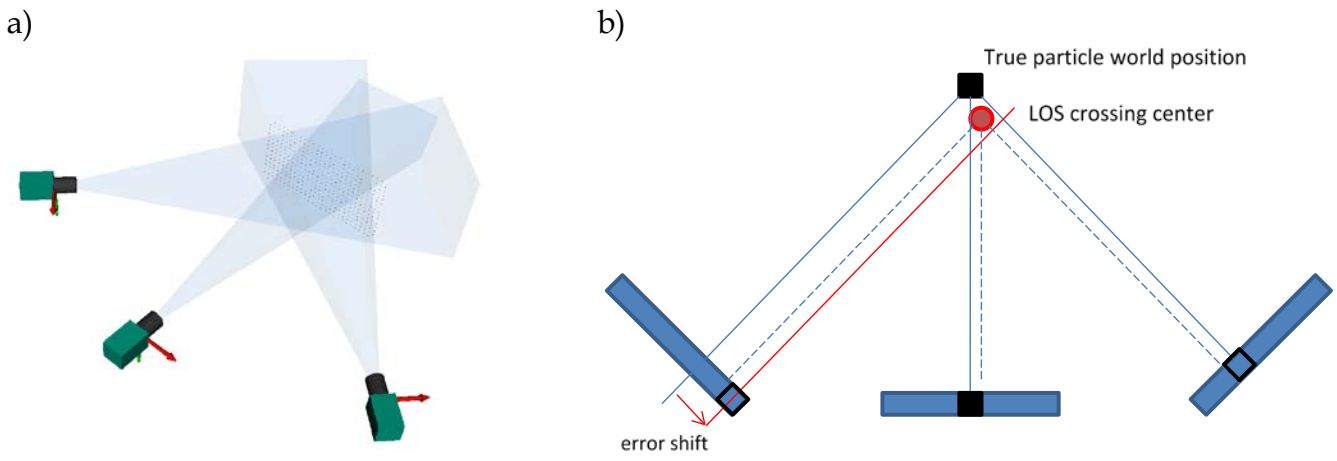

Fig. 1: Camera configuration for volumetric reconstruction; a) typical camera arrangement in different planes, b) camera arrangement in the horizontal plane with illustration of perfect calibration and with mismatch due to an in-plane shift of the left camera. Blue filled rectangles represent the image planes. Blue solid lines show the LOS for perfect calibration crossing in the true particle world coordinate in the center of gravity. Black squares show the particle image projection in the image planes. An error introduced on the left cam#1 by an in-plane shift (red arrow) leads to a new center in the reconstruction (red circle) dislocated away from the original position. Corrections for perfect crossing of the LOS affects all cameras seen by the disparity shift of the blue dashed lines. Hence, the mismatch correction can be done either correcting only cam #1 or all cameras simultaneously.

The blue solid lines show the LOSs for perfect calibration crossing in the true particle world coordinate system in the center of gravity. An error introduced on the left cam#1 by an in-plane shift (red arrow) leads to a new center in the reconstruction (red circle) dislocated away from the original position. Corrections in form of disparity maps can either be applied only to cam#1 or to all cameras together simultaneous (shown by the dashed blue lines). Note that both methods lead to perfect mapping, however the world coordinate system as a whole may translate relative to the cameras.

Particle representation in reconstructions with mismatch

The misalignments of the LOS lead to a change of the intensity distribution of the MART or SMART reconstruction with a resulting shift of peak intensity location or - in SOS - a shift of the center of gravity, see Fig. 2. The fact used herein is that for Gaussian particle images and disparities smaller than their diameter, the voxel reconstruction of the particle remains well represented by a Gaussian blob of nearly spheroidal shape (ideally a sphere). This is demonstrated in a simulation of a synthetic Gaussian blob with 30vx diameter in a voxel volume, representing a situation of a ten-fold super-resolution of a 3px diameter particle.

.

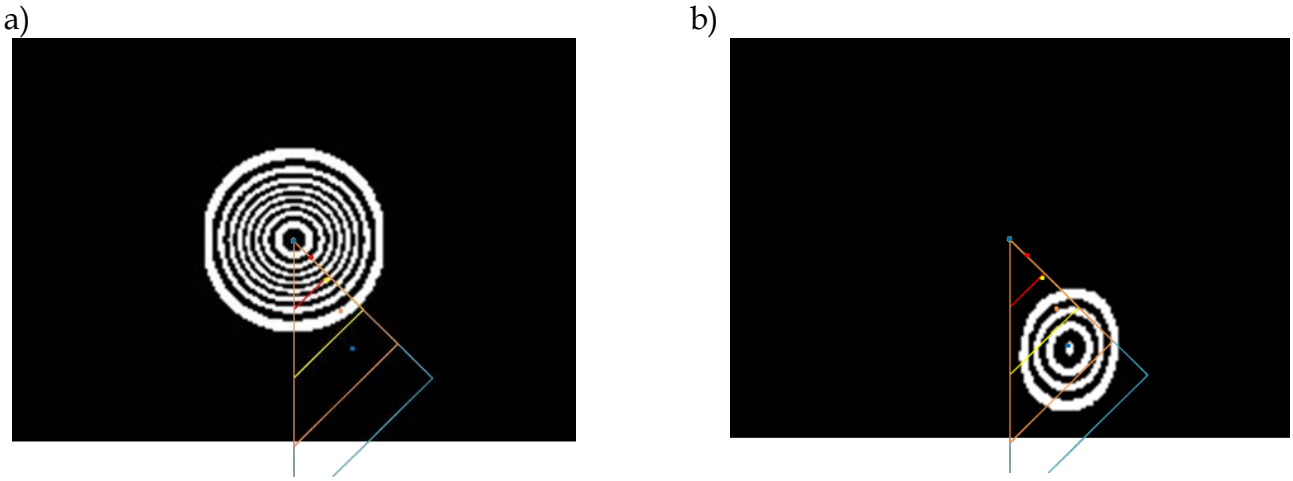

Fig. 2: Topview on the MART reconstruction of a simulated particle with artificially enlarged dP=30px diameter and Gaussian intensity distribution, visualized via iso-lines of grey levels, using the camera configuration shown in Fig. 1b. a) zero mismatch, b) after disparity shift in the left camera cam#1. Note the shift of the intensity maximum in the reconstruction away from the original center. The triangles indicate the LOSs starting at the particle image centers for different pixel disparities of cam#1 (blue: 1dP, brown: 3/4dP, yellow: 1/2dP, red: 1/4dP). The colored dots indicate the locations of maximum intensity for the different disparities.

The up-scaling is done herein to highlight the intensity distribution of the reconstruction. We assume perfect linear mapping functions (straight LOS) and calculate the back-projections of the Gaussian blob onto the image planes. Then, we shift the image in the left camera cam#1 stepwise to introduce a calibration error and reconstruct the voxel volume again. The result given in Fig. 2 is shown in the horizontal center-plane of the reconstruction. In order to highlight the shape of the intensity distribution and the location of the peak, the images are shown as contours of constant intensity with constant incremental value.

In case of perfect calibration (zero mismatch), see Fig. 2a, the blob has a spherical structure (circular in the top-view) of Gaussian intensity distribution with the maximum very close to the geometric crossing of the LOSs through the center of the particle images. Once the left camera cam#1 is misaligned about a number of pixels to the right, this reconstruction deforms into an elliptical shape with the intensity maximum shifted away from the original center, see Fig. 2b. Despite a shift in cam#1 of order of one particle diameter, the simulations show that the reconstruction still provides a compact spheroidal contour with approximate Gaussian intensity distribution. This fact allows us to use sub pixel analysis in the following correction step. The simulations for different disparity shifts also show that the locations of maximum intensity in the reconstruction remain always in the inner part of the triangle defined by the LOSs through the particle image centers.

Back-projection and cross-correlation

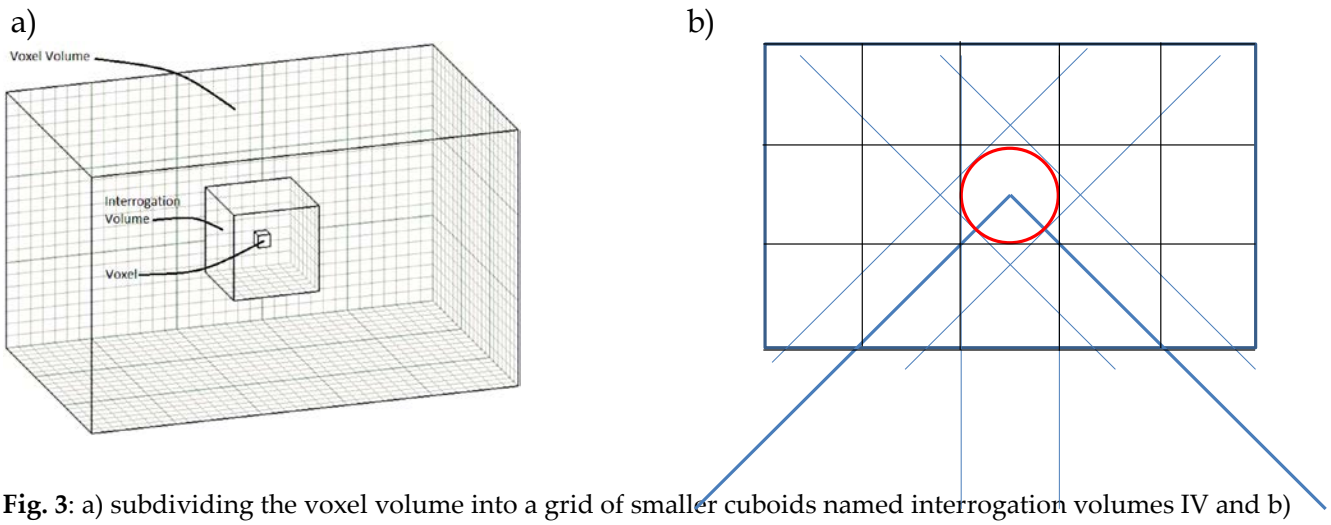

Fig. 3: a) subdividing the voxel volume into a grid of smaller cuboids named interrogation volumes IV and b) masking a spherical box around the center of the IVs (red circle in top view) prior to back-projection of the IV into the image planes. This ensures that only those voxels inside the spherical volume of the IVs are contributing to the intensity in the projections.

The reconstructed voxel volume is divided into different Interrogation Volumes (IV) and each IV is projected back into the image plane of all cameras. Prior to projection into the image planes, all voxels outside of the sphere with diameter of the IV are set to zero (red circle in Fig. 3b) so that the back-projection in the image plane is built only from intensities of voxels inside the IV. The image contains then a circular region of gray-level pixels, centered to the location of the IW-center projected into the image plane. This is the template window IWbp, which stands for "interrogation window in back-projected image of IW". A corresponding interrogation window IWim is selected at the same location in the original images (IWim stands for interrogation window in original image). The calibration mismatch is assumed as a smooth function in space leading to approximately a linear translational shift locally in the IWbp relative to the IWim. This shift vector can be calculated from 2D cross-correlation between both windows. Because of preservation of gaussian intensity distribution in the reconstructions and back-projections even under larger disparity as shown above, this shift can be determined with sub-pixel accuracy in the image plane.

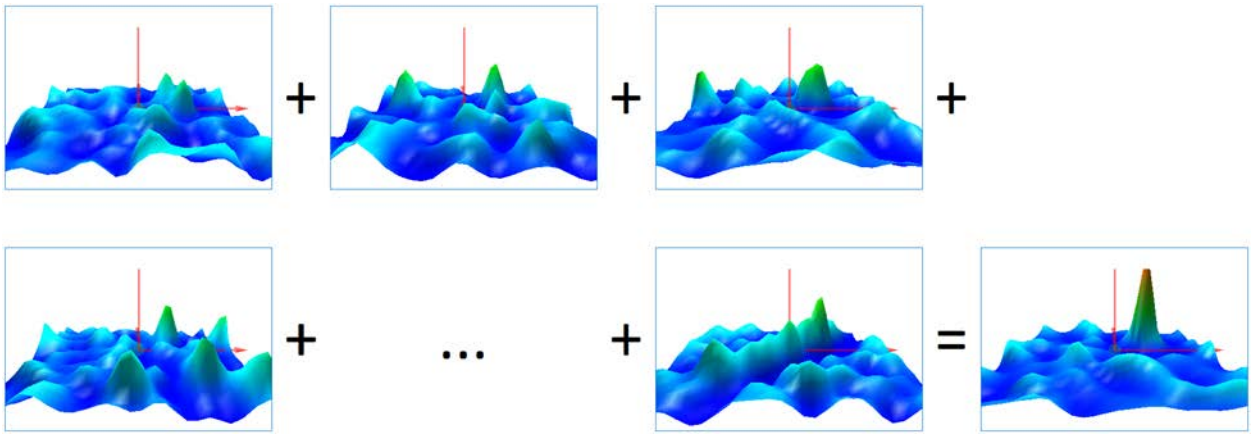

Fig. 4: Addition of the correlation maps for the same IV and camera, obtained from different sets of particle images. The resulting peak represents the disparity shift in the image plane for the given center-location of the IV in the reconstructed voxel volume.

Note that the IWim in the image plane can contain particle images, which result from locations in front or behind the IV along the viewing direction of the camera, see Fig. 4. The probability increases with increasing particle number density. This effect together with other contributions such as ghost particles or image noise lead to the fact that the particle images in the IWim and the particle images of the IWbp from the masked back-projection cannot match perfect. On the other hand, the calibration mismatch introduces a systematic shift, independent on the statistical

properties of ghosts or noise. Therefore, we use several realization of particle images and store the cross-correlation maps for each IV. The corresponding correlation maps at each IV center are then added, see Fig. 4, and finally the peak in the sum of the correlation maps is calculated with subpixel accuracy. This value is stored as disparity vector for each camera and each IV center location in the voxel volume. The core of the procedure to correct the mismatch is summarized in the following chart Fig. 5.

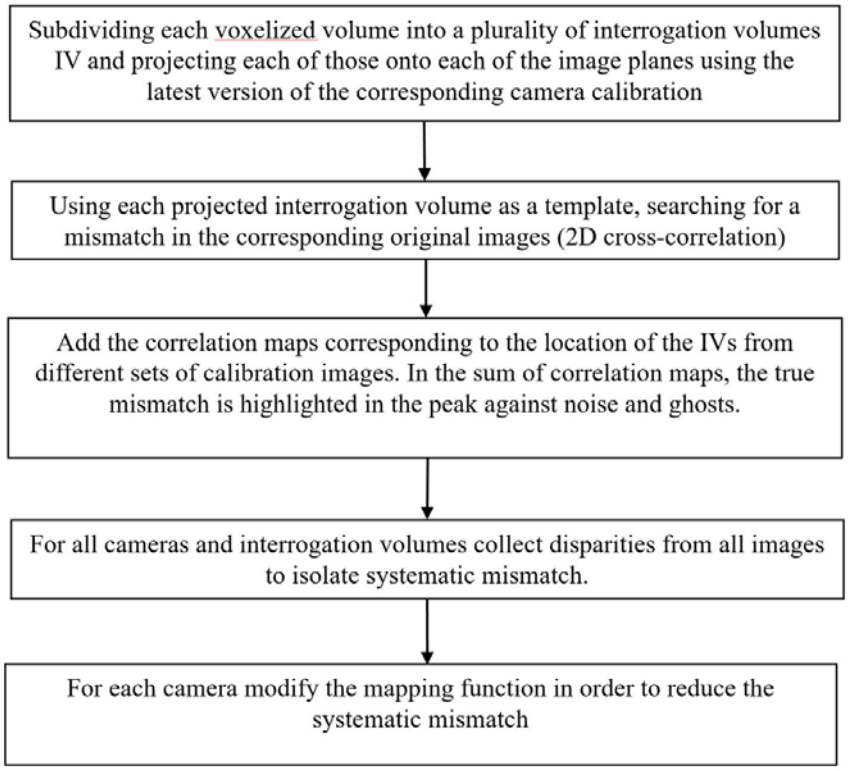

Fig. 5: Flow chart of the major part of the correction methodology

Correction steps and convergence

The analyzed disparities are then used to correct the initial calibrations by updating the mapping functions. Synthetic particle fields are generated to test the convergence of the iterative procedure. To simplify the simulation, a thick voxel sheet (depth 160 vx, width 225 vx, height 5vx) is generated and filled randomly with Gaussian blobs of diameter 3vx to generate particle images with a density of 0.02ppp. All centers of the particles lie in the horizontal mid plane at a height of 3vx. The initial mapping function assumes straight parallel LOS normal to the image planes (telecentric conditions) at magnification of 1 without any optical distortion. First, the LOSs are determined

and the corresponding images of the camera setup (Fig. 1b) are generated by back-projection. The ground truth is then the MART reconstruction from these images (the ground truth therefore can already contain ghost particles, if particle density is high). In a second step, a shift is introduced on cam#1 as indicated in Fig. 1b and a new voxel volume is reconstructed based on this mismatch. The shift can be understood either as a misalignment of the camera after calibration or equivalently as an error in the original mapping function of cam#1. To correct this, the volumetric calibration refinement procedure is started by back-projection of the masked IVs and cross-correlation is done with the IWbp and IWim in the original (zero-shifted) images. The same procedure can be repeated with different random arrangements of particles in the voxel sheet such that 10 correlation maps exist for each IV, which then can be summed up. However, as the LOSs are straight parallel lines and the shift is constant over the entire image of cam#1, the number of 10 IVs in one reconstruction allows to get the added correlation maps just from one single simulation.

The resulting peak-locations in the added correlation maps correspond to the disparities in the different cameras. As seen in Fig. 1b, the corrections for perfect crossing of the LOS can affect all cameras illustrated by the disparity shift of the blue dashed lines in Fig. 1b. Hence, the mismatch correction can either be done correcting only cam#1 or all cameras together simultaneous. Fig. 6 shows the iterative correction procedure if only cam#1 with the largest disparity is corrected after each step. The initial shift of cam#1 is 3px in positive direction of the long axis of the image, see Fig 1b. After the first step of correction, the disparities from the added correlation maps result to values of -1.1 for cam#1, +0.5px for cam#2 and 0 for cam#3. Hence, the largest correction is for cam#1 to achieve a better match of the back-projections with the original images. Interestingly, cam#3, which is looking perpendicular to the view of cam#1 where the error shift is introduced, has a zero disparity. This is expected as the error shift vector is parallel to the viewing direction of cam#3. Now, the initial error shift of 3px on cam#1 is correct with a disparity of -1.1px, while all other original image are not changed. Thus, we generate a new image of cam#1 with an error shift of +1.9px (+3px-1.1px) in direction of the long axis compared to the original image. This is equivalent to updating the mapping function of cam#1 after the first iteration step.

Further correction steps are done in the same way until the final residual compared to the original image is less than 0.1px. The resulting iteration steps with the correction values of all cameras are given in Fig. 6. Note that the largest disparity remains in all steps for cam#1, which is the one where the calibration mismatch was introduces in form of an error shift. The correction steps lead to a mismatch of cam#1 from the original shift of +3px in step 1 to +1.9px (+3px -1.1px), in step 2

to +1.1px (+3px -1.1px -0.8px), in step 3 to +0.5px (+3px -1.1px -0.8px -0.6px), in step 4 to +0.1px (+3px -1.1px -0.8px -0.6px -0.4px) and finally in step 5 to 0 px (+3px -1.1px -0.8px -0.6px - 0.4px - 0.1px). That means the image of cam#1 with the imposed 3px error shift has been shifted back to the original image after 5 iteration steps and the mapping functions now correspond to a perfect calibration.

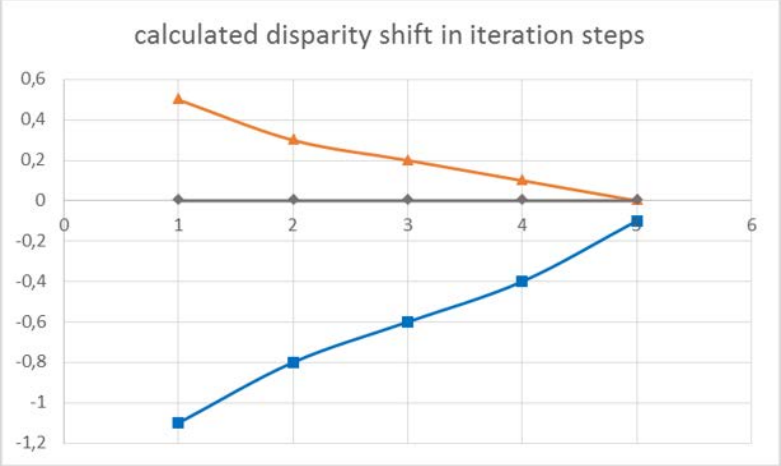

Fig. 6: Iterative reduction of residual disparity shifts in all three cameras after inducing an initial 3px mismatch in cam#1 in positive direction along the long axis of the camera, see Fig 1b (blue: cam#1, orange: cam#2, gray: cam#3).

Fig. 7 shows the reconstructions of particle fields starting from a +3px mismatch along the long axis of cam#1 before and after the final correction step (top-view of the MART volume) of the error shift indicated in Fig 1b. Due to the mismatch of cam#1 representing a systematic error in the mapping function of cam#1, the reconstruction shows a larger number of ghosts near original particle images. Note that the original images were blurred with a 3x3 Gaussian kernel prior to reconstruction to highlight this effect. After the final correction step, all original particles are reconstructed in their true shape and location and no ghosts are seen.

The method has been further tested for synthetic images including noise and has been proven robust and practicable. For most cases, a total number of 5 iteration steps is sufficient to reduce the residual below 0.1px. Note that the number of iterations depends on the number density of particles in the calibration images and the number of IV in the total volume. The latter needs also a sufficient grid resolution so that the determination of improved transfer functions can cope with camera rotation, translation and optical distortions. A practical number is about 5x5x3 IV in a typical volume. Though, it is recommended to keep the number of IV constant with the aspect ratio of the volume.

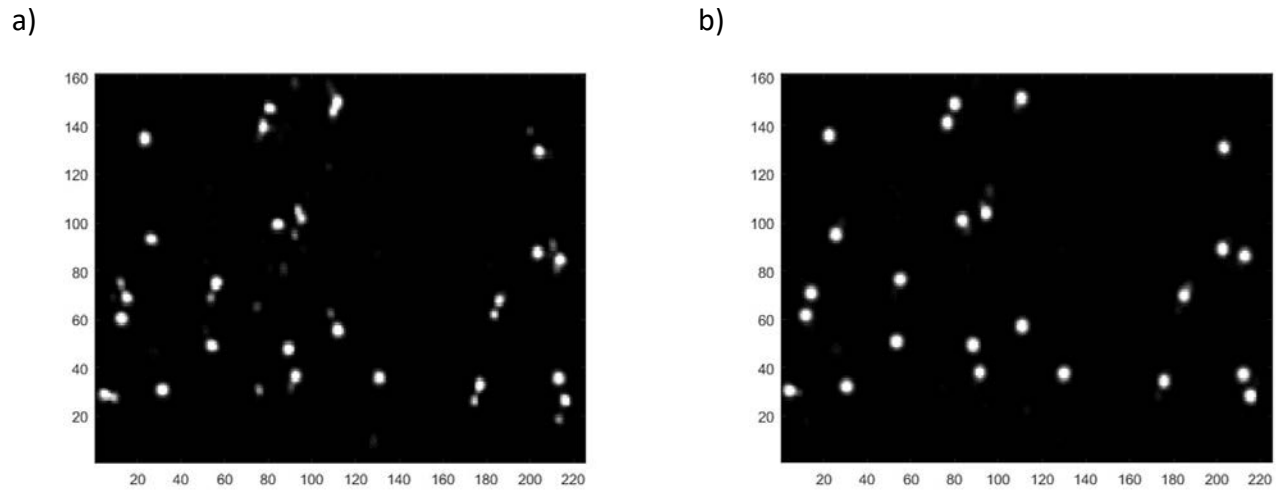

Fig. 7: Top view of MART reconstruction of particle field in the three-cam arrangement shown in Fig. 1. a) reconstruction with initial error in calibration with 3px error shift in cam#1, showing larger number of ghosts. b) reconstruction after final iteration step in Fig. **6**.

3. Synthetic data analysis

In order to judge about the quality of this refinement method under more realistic conditions, a complete experiment with optical transfer functions including noise and lens distortion is simulated. In the first step, the initial calibrations of the original camera positions are defined and used for the calculations of the LOSs and back-projection of randomly distributed particles in the voxel volume. In the second step we simulate a sparse set of particle images, where the camera positions are modified and the images are distorted. These images are used for calibration refinement. Afterwards, the initial and the refined calibrations are used to reconstruct voxel spaces for dense particle fields at different time-steps of a given stationary flow field. In a final step, the velocities of the different reconstructions can be analyzed by 3D Least Squares Matching (3D LSM, see Westfeld et al 2010). Thus the resulting vector-maps of the refined and non-refined calibrations can be compared and improvements can be quantified.

Four synthetic cameras (800x500pixels) are arranged in a cross-type configuration, observing a segment of a Hill-type ring vortex in a volume of 65x45x15 mm. This set-up also represents the initial calibration. The volume is reconstructed in isotropic voxels of 0.1mm length, totaling in 650x450x150 vx. To introduce an error, the cameras are moved away from their theoretical initial position in the following way: the top and right cameras are moved up by 0.5 mm; similarly, the

bottom and the left cameras are shifted 0.5 mm to the right. With a magnification factor of 1 pix = 1 vox = 0.1 mm, each camera is moved with a shift of 5 pixel. Additionally, distortions are added to the images by the radial parameters of the pinhole camera model. This distortion introduces a maximum shift of additional 1.5 pixel, summing the maximum potential calibration error to more than 9 pixel.

For the calibration refinement process, a set of particle images with moderate particle density is simulated. To better represent an experimental environment, noise is added to the images. The maximum particle gray values are in the range of 35 counts to represent a low light situation, the added noise level is 6 counts with a standard deviation of 2 Sigma. During image pre-processing steps, the noise is reduced by a local average subtraction, a threshold and final Gaussian smoothing with a 3x3 kernel. For processing the refined calibration, a set of 10 images is used. The number of cuboidal IVs for the correlations is set to 10x6x3 with each IV of the size of a cuboid of 80vx length. This results in one disparity vector every 63rd voxel in x- and y axis and every 35th voxel in z-direction, respectively. Note that for the z-direction the IVs are overlapping each other. For the refinement, all cameras were corrected at the same time in each iteration.

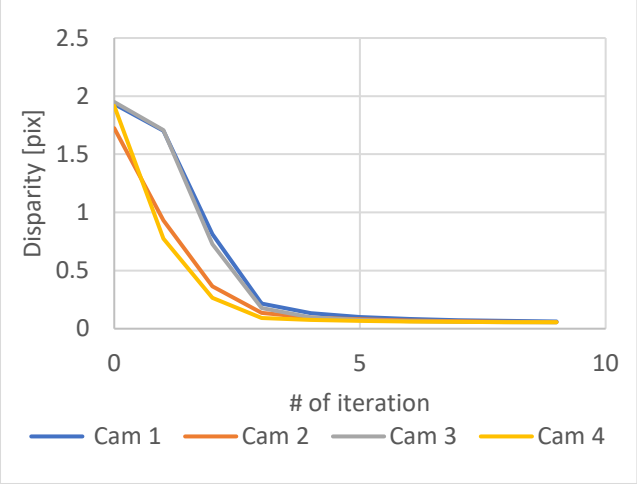

Fig. 8: Average disparity error over the number of refinement iterations

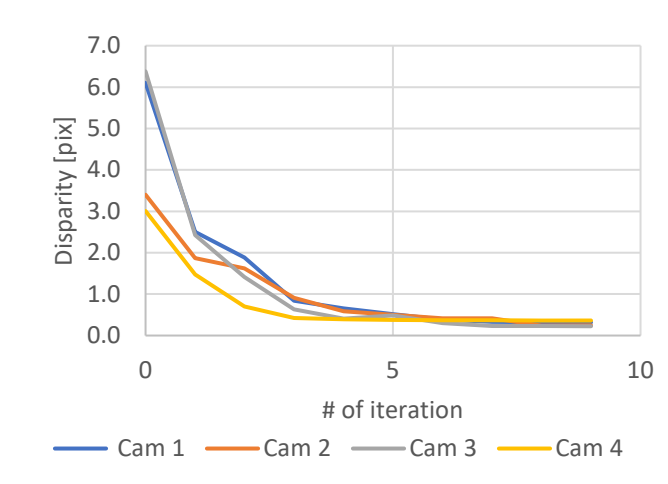

Fig. 9: Maximum dispartiy error over the number of refinement iterations

The results of the refinement shows that within 5 iterations the average projection error drops from 1.88 pixel to 0.1 pixel and the maximum disparity is reduced from 6.4 to 0.5 pixel (see also Fig. 8 and Fig. 9). After 10 iterations, the maximum disparity is about 0.36 pixel and the average disparities are 0.057 pixel. This is by far less than the required 0.4 pixel of uncertainty claimed by Arroyo and Hinsch in 2008 and in the same range as described by Wieneke in 2008.

In the final step, the refined calibrations are used for volume reconstruction and are compared with the initial calibration as well as with a simulated volume of the known particle positions.

Fig. 10: Z-axis intensities of the reconstructed voxel spaces indicates the large improvement in ghost level intensities between the reconstructions with the outdated initial- (red line) and the reconstruction using the refined calibration (yellow line).

Fig. 10 shows the intensity profiles along the z-axis of the voxel space. The normalized signal level in the illuminated area -7.5 < z < +7.5 mm is about 0.87, and the average normalized noise level is about 0.65. This results to an average signal to noise ratio (SNR) of 1.3. For the enhanced calibration, the values are about 0.85 for the signal level and about 0.085 for the noise level, resulting in an SNR of about 10. Hence, the reconstruction using the volumetric calibration offers more than 7 times higher signal quality. The benefit of lower ghost level intensities after refinement has been discussed, for instance, by Novara et al (2010) and de Silva et al. (2012). A side effect of the refinement is a shift of the z-location of the measurement domain as discussed above and also discussed by Cornic et al. (2015), which makes a voxel-wise comparison difficult.

The direct impact of the enhanced calibration on the 3D velocity measurements is shown by processing the displacements in three successive particle volumes in time. The method of 3D Least Squares Matching (3D LSM) was applied on the synthetic voxel space as well as the two reconstructed ones. Fig. 12 shows the results. Here, the yellow-colored vectors are from the voxel spaces that used the refined calibration and show a clear improvement over the vector quality against the red-colored vectors from the analysis with the initial calibration. Furthermore, the

yellow-colored vectors are in good agreement with the velocities obtained from the simulated voxel space (green-colored vectors).

Fig. 11: comparison of z-axis intensity profiles in the 3 different voxel-spaces. Red: Voxel space from initial calibration. Green: Voxel space from simulated voxel space. Yellow: Voxel space from refined calibration.

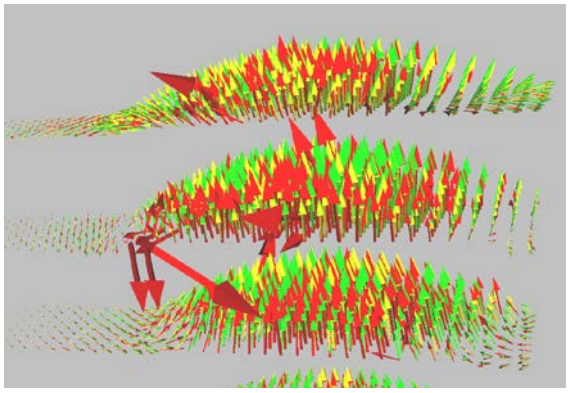

Fig. 12: Simulated comparison vector results demonstrate the improvement Volumetric Calibration Refinement. Red: Velocities from outdated initial calibration. Green: Velocities from simulated voxel space. Yellow: Velocities from refined calibration.

Though, the green and the yellow vector fields look similar in both direction and magnitude, as seen with other refinement methods (Cornic et al. 2015), the coordinate system of the refined calibration gets slightly shifted away from the original during the refinement step. This makes a direct comparison of the vectors from the refined calibration and the simulated ones difficult.

4. Experimental data analysis

For the experimental case, a transitional water jet-flow is used. The jet emits from a nozzle with diameter (D) of 12.36 mm at a flow rate of 100 l/h, resulting in an average flow velocity at the orifice of approximately 0.232 m/s. With the given velocity and viscosity, the Reynolds number is approximately 3000. The flow is measured by a set of 4 Speed-Sense M 310 (1280x800 pix) cameras in an inline configuration up to 4000 individual images that were illuminated by a DualPower 30-1000 Laser and recorded with a repetition rate between 800 and 1200 Hz.

A volume of 27 x 65 x 27 mm is reconstructed with the initial calibration and with a refined calibration. The result of the z-axis intensities can be found in Fig. 13 . An improvement of the signal to noise ratio can be observed again, though it is not as pronounced as in the synthetic simulated data fields. Comparing the vectors in Fig. 14 also shows a reduced number of outliers

between the red-colored ones where the reconstruction was based on the initial calibration, compared to the reconstruction with the refined calibration (yellow-colored vectors).

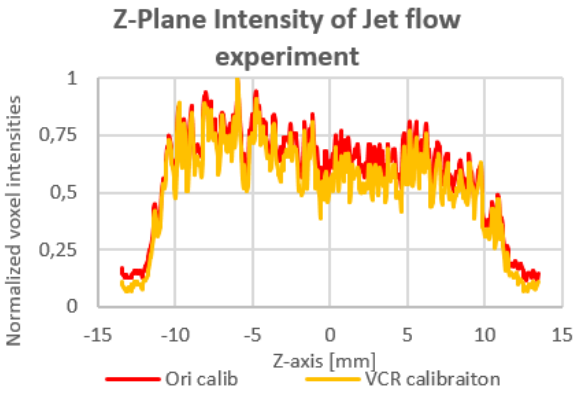

Fig. 13: Comparison of average z-plane intensity of the jet flow experiment. Red - with initial calibration, yellow - with VCR.

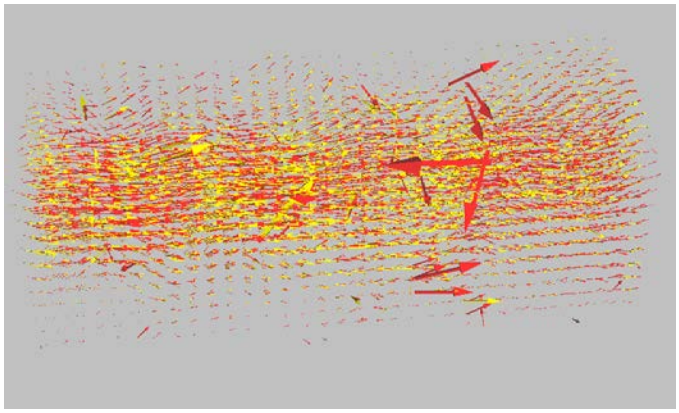

Fig. 14: Comparison of vectors with the initial calibration (red) and with VCR (yellow).

5. Summary

This study presents a new approach to enhance a 3D camera calibration based on particle images, which is based on a statistical approach of reconstructed particles in sub volumes (Interrogation Volumes IV) and their masked back-projected images in the image planes. The initial total volume, represented as a voxel-based grid, is generated from the parameters of an initial classical multi-camera calibration. This volume is subdivided into smaller cuboids for each of which a back-projection into the camera planes is calculated. Voxels outside of the IV are blanked out and the resulting back-projections are compared with the original images around the location of the center of the IV projected back into the image plane. Cross-correlations between both image regions (back-projected IWbp and original IWim) and successive adding of the correlation maps of different realizations of calibration experiments then leads to accumulated peaks in the maps which represent the average disparity, assigned to the centers of the IVs. The calibration parameters are then corrected in an iterative procedure improving the transfer functions between image- and world coordinates. The process converges after 5-10 iteration steps down to residual disparities less than 0.1 px for all cameras, based on simulations with synthetic images. The new method is robust and practical in its use as it does not require any user input and can be automatized with a given set of design rules.

The study of the entire process from calibration over the volumetric reconstruction to the final vector analysis using 3D LSM routines shows a great potential of the new refinement method. In the synthetic case, a disparity of more than 9 pixels in length was corrected to an average disparity error in the range of 0.05 pixel, despite the simulated added noise of the simulated particle images. When comparing the reconstructed voxel volumes, a clear advantage can be seen. The z-intensity profiles of the different volumes show that the SNR improved over 7 times when the refined calibrations are used instead of the initial calibrations. Hence, the reconstruction quality is drastically improved. Comparing the 3D-LSM results of the volumes from the initial calibration and the refined calibrations, a clear reduction in erroneous vectors is seen. Furthermore, comparing the improved results with the 3D-LSM results obtained for ideal simulated voxel spaces, a good agreement of the vectors is obvious. Though, similar as with other refinement methods, the coordinate systems gets slightly shifted making it difficult to directly compare the vector results.

References:

Arroyo P, and Hinsch K (2008) "Recent Developments of PIV towards 3D Measurements"; In The PIV book: A. Schroeder, C.E. Willert (Eds.): Particle Image Velocimetry, Topics Appl. Physics 112, 127–154 (2008) © Springer-Verlag Berlin Heidelberg 2008

Atkinson C H, Soria J: (2007) "Algebraic Reconstruction Techniques for Tomographic Particle Image Velocimetry" 16th Australasian Fluid Mechanics Conference, Australia 2-7 December 2007

Cornic P, Illoul C, Le Ant Y., Cheminet A., Le Besnerais G, Champagnat F: (2015) " Calibration drift within a Tomo-PIV setup and Self-Calibration"11TH INTERNATIONAL SYMPOSIUM ON PARTICLE IMAGE VELOCIMETRY – PIV15 Santa Barbara, California, September 14-16, 2015

de Silva C M, Baidaya R, Marusic I: (2012) "Enhancing Tomo-PIV reconstruction quality by reducing ghost particles" Meas. Sci. Technol. 24 (2013) 024010

Novara M, Batenburg K.J., Scarano F: (2010) "Motion tracking-enhanced MART for tomographic PIV" Measurement science and technology, 21 (3) 2010

Westfeld P, Maas H G, Pust O, Kitzhofer J, Brücker C: (2010) "3D least square matching for volumetric velocity data processing" Proc. 15th Int. Symp. on Applications of Laser Techniques to Fluid Mechanics (Lisbon, 5–8 July 2010) 3.7

Wieneke B, (2008): "Volume self-calibration for 3D particle image velocimetry" Exp Fluids (2008) 45:549–556, DOI 10.1007/s00348-008-0521-5